APPLIED RESEARCH

Current Controller Based on Active Disturbance Rejection Control With Parameter Identification for PMSM Servo Systems

SHANGYAO SHI[1], LUJI GUO[2], ZHE CHANG[2], CHENBO ZHAO[2], AND PENGYUN CHEN[2]

[1]School of Software, North University of China, Taiyuan 030051, China
[2]School of Aerospace Engineering, North University of China, Taiyuan 030051, China

Corresponding author: Pengyun Chen (chenpengyun@nuc.edu.cn)

ABSTRACT This study aimed to design an active disturbance rejection control (ADRC) with parameter identification for current control in permanent magnet synchronous motor (PMSM) servo systems. Given the nonlinear uncertainty of the PMSMs, a parameter identification method based on the consensus Kalman filter was designed to establish an approximate model of the motor, reduce the uncertainty of the current loop model, and utilize the improved ADRC algorithm to eliminate the influence of uncertainty, nonlinearity, and strong coupling of the current loop of the PMSM. Consequently, the current control precision of the inner loop improved. The control experiment results indicate that the proposed method is suitable for the current control of nonlinear and strongly-coupled servo systems.

I. INTRODUCTION

Permanent magnet synchronous motors (PMSMs) are widely used in servo systems owing to their high power density, high efficiency, and small inertia [1], [2], [3]. Hence, the control technology of these systems comprising PMSMs has become a research hotspot [4]. The PMSMs are characterized by time-varying parameters, strong coupling, and variable nonlinearity, and their control strategy directly influences the control effect. Generally, servo systems use the nested structure of the current, speed and position loops, and the performance of the outer loop depends on the optimization of the inner loop [5]. As an innermost loop, the current control is directly related to the output electromagnetic torque. Hence, its dynamic and static performance is directly related to the performance of the position servo system [6], [7]. PMSMs exhibit advantages such as high power factor, high efficiency, and wide

The associate editor coordinating the review of this manuscript and approving it for publication was Zheng H. Zhu.

speed range, and they are widely used in electric vehicles, oil exploitation and military equipment industries [8].

The current loops mainly use proportional–integral (PI) [9], hysteresis [10], sliding mode [11] and predictive control [12] methods, which have advantages and disadvantages. The hysteresis control has a fast response. However, its disadvantages include current ripples and steady-state errors owing to the variable switching frequency [13]. The sliding mode control is characterized by fast speed and strong robustness but has a 'chattering' problem [14]. Predictive control can realise the fast-tracking of the command signal without overshoot; however, it relies on the precision of the mathematical model of the controlled object and lacks robustness. The PI controllers, which have simple structures and exhibit stable performance, are the most widely used control algorithm in current loops [15], [16], [17]. However, they exhibit difficulties balancing between speed and overshoot, and integral saturation problems. Additionally, for the small inertia position servo system, the speed changes frequently,

and the electromagnetic time constant is equivalent to the electromechanical time constant. Hence, the back electromotive force (EMF) interference cannot be ignored, thereby annulling the applicability of the conventional PI control. Owing to the uncertainty of the flux parameters, the quality of the speed signals and loop delay, the direct feedforward compensation method of the back-EMF based on the conventional PI control remains impractical in engineering. Further, time delay in the digital control process causes the control input and controlled variable to change asynchronously. When the controller gain is not properly selected, overshoots and possibly system oscillations are inevitable. Based on the limitations of the conventional PI control, the improvement measures such as feedforward compensation, anti-integral saturation and fuzzy PI controls have been proposed, thereby achieving excellent results. Particularly, active disturbance rejection control (ADRC) [18], [19] was proposed, which significantly overcame the limitations of the PI control and achieved promising control performance. ADRC has been employed in speed and position loops although its application is limited in current loops.

The parameters of a PMSM change with changes in the working condition, service time, and load. Thus, the motor parameters of the PMSM should be identified online, approximate model of the motor established, internal disturbances (model errors) reduced, system uncertainties reduced, "time scale" of the system increased [20], burden of the motor controller lightened and observation and control bandwidth of the system improved. First, this study established the mathematical model of the PMSM. The PMSM system was proven to be an observable and controllable flat system. Thus, a parameter identification method based on the consensus extended Kalman filter (CEKF) [21] was proposed. Combined with the EPADRC algorithm [22], a current control method with a parameter identification function for the PMSM servo system is proposed, thereby eliminating the influence of the uncertainty (model error and external disturbance), nonlinearity and strong coupling of the PMSM current loop, and improving the current control accuracy of the inner loop. Based on control experiments, the proposed method can track the reference input current quickly, accurately, and without overshoot. Additionally, it has better dynamic characteristics and robustness compared to the existing ADRC control.

II. PMSM MOTOR MODEL

The rotor of the PMSM is either surface-mounted or embedded depending on the structure. In this study, the back EMF of the three-phase symmetrical stator winding of the PMSM is a sine wave. The three-phase sine wave current with a phase difference of 120° must be passed through the stator winding of the motor to produce continuous electromagnetic torque. Currently, the permanent magnet of the rotor of the PMSM generates a rotating magnetic field, which is similar to a sine wave in the air gap based on the principle of electromagnetic induction. Sira-Ramirez et al. [23] and Louis [24] discussed the model of the PMSM and control

background and method of the PMSM, respectively. At α-β in the stationary coordinate system, the mathematical model of the PMSM is expressed as follows:

$$\begin{cases} u_\alpha = R_s i_\alpha + \dfrac{d\psi_\alpha}{dt} \\ u_\beta = R_s i_\beta + \dfrac{d\psi_\beta}{dt} \end{cases} \tag{1}$$

where α and β are constants. The axial flux linkage is expressed as follows:

$$\begin{aligned} \psi_\alpha &= L_\alpha i_\alpha + \psi_r \cos(n_p \theta_e) \\ \psi_\beta &= L_\beta i_\beta + \psi_r \sin(n_p \theta_e) \end{aligned} \tag{2}$$

Then there are

$$\begin{cases} L_\alpha \dfrac{di_\alpha}{dt} = u_\alpha - R_s i_\alpha + n_p \psi_r \omega_e \sin(n_p \theta_e) \\ L_\beta \dfrac{di_\beta}{dt} = u_\beta - R_s i_\beta - n_p \psi_r \omega_e \cos(n_p \theta_e) \\ J \dfrac{d\omega_e}{dt} = T_e - B\omega_e - T_L \\ \dfrac{d\theta_e}{dt} = \omega_e \end{cases} \tag{3}$$

In equation (3), u_α, u_β Respectively α, β Input voltage on the shaft; i_α, i_β Respectively α, β Phase current on the shaft; L_α, L_β PMSM in the α, β Inductance on the shaft; R_s is the phase resistance on the PMSM stator winding; T_e and T_L are the electromagnetic and load torques of the PMSM, respectively, B is the frictional damping coefficient, ψ_r is the flux linkage of the permanent magnet of the PMSM, n_p is the number of pole pairs of the PMSM, ω_e is the mechanical rotational speed, θ_e is the absolute angular position of the PMSM rotor. The absolute angular position of the motor rotor θ_e, initial angular position of the motor rotor θ_0, measured angular displacement of the motor rotation angle θ, electrical angular velocity of the motor ω_r and mechanical angular velocity ω_e are related as expressed below:

$$\begin{cases} \theta_e = \theta_0 + \theta \\ \omega_r = n_p \omega_e \end{cases} \tag{4}$$

The vector control algorithm and direct torque control algorithm of the PMSM control the current and voltage of the stator winding in the d-q rotating coordinate system, respectively. The mathematical model of the PMSM in the rotor synchronous rotating d-q coordinate system can be obtained via the following coordinate transformation:

$$\begin{cases} \begin{bmatrix} i_d \\ i_q \end{bmatrix} = \begin{bmatrix} \cos(n_p\theta) & \sin(n_p\theta) \\ -\sin(n_p\theta) & \cos(n_p\theta) \end{bmatrix} \cdot \begin{bmatrix} i_\alpha \\ i_\beta \end{bmatrix} \\ \begin{bmatrix} u_d \\ u_q \end{bmatrix} = \begin{bmatrix} \cos(n_p\theta) & \sin(n_p\theta) \\ -\sin(n_p\theta) & \cos(n_p\theta) \end{bmatrix} \cdot \begin{bmatrix} u_\alpha \\ u_\beta \end{bmatrix} \end{cases} \tag{5}$$

The differential equation of the PMSM in the d-q rotating coordinate system is expressed as follows:

$$\begin{cases} L_d \dfrac{di_d}{dt} = u_d - R_s i_d + n_p \omega_e L_q i_q + n_p \psi_r \omega_e \sin(n_p \theta_0) \\[2mm] L_q \dfrac{di_q}{dt} = u_q - R_s i_q - n_p \omega_e L_d i_d - n_p \psi_r \omega_e \cos(n_p \theta_0) \\[2mm] J \dfrac{d\omega_e}{dt} = T_e - B\omega_e - T_L \\[2mm] \dfrac{d\theta_e}{dt} = \omega_e \end{cases}$$

(6)

The initial angle $\theta_0 = 0$. Here, the angular position is similar to the angular displacement and (6) can be expressed as

$$\begin{cases} L_d \dfrac{di_d}{dt} = u_d - R_s i_d + n_p \omega_e L_q i_q \\[2mm] L_q \dfrac{di_q}{dt} = u_q - R_s i_q - n_p \omega_e L_d i_d - n_p \psi_r \omega_e \\[2mm] J \dfrac{d\omega_e}{dt} = T_e - B\omega_e - T_L \\[2mm] \dfrac{d\theta_e}{dt} = \omega_e \end{cases}$$

(7)

The electromagnetic torque of the PMSM can be expressed as $T_e = 1.5 p_n [\psi_r i_q + (L_d - L_q) i_d i_q]$. According to Shi et al. [20], one system is expressed as follows:

$$\dot{x} = f(x, u) (x \in R^n, u \in R^m) \qquad (8)$$

A dummy output variable $y = (y_1, \cdots, y_m)$ can be represented using a state variable x and control output u. The finite subdifferential term is generally represented as

$$\begin{cases} x = A(y, \dot{y}, \cdots, y^{(\alpha)}) \\ u = B(y, \dot{y}, \cdots, y^{(\beta)}) \end{cases} \qquad (9)$$

Similarly, the virtual output variable y can also be represented by the state variable x and control output u. The finite-order differential term of a real analytic function is generally expressed as

$$y = C(x, u, \dot{u}, \cdots, u^{(\gamma)}) \qquad (10)$$

Thus, equation (8) is considered a differentially flat system, which can be linearized by internal feedback. Here, y can be viewed as a virtual output (also known as linear or planar output). From equations (9) and (10), a major characteristic of a flat system is that the state variable x and input variable u can be directly output by the flat output y and its finite-order differential explicit expression, thereby showing that the state variables of the system can be monitored and controlled. According to Michel et al. [25], if θ and i_d are flat outputs,

the PMSM model can also be expressed as follows:

$$\begin{cases} i_q = \dfrac{J}{K_m} \ddot{\theta} + \dfrac{B}{K_m} \dot{\theta} + \dfrac{T_L}{K_m} \\[2mm] u_q = \dfrac{L_q J}{K_m} \dddot{\theta} + (\dfrac{L_q B + R_s J}{K_m}) \ddot{\theta} + n_p L_d i_d \\[2mm] u_d = L_d \dfrac{di_d}{dt} + R_s i_d - n_p \dot{\theta} L_q (\dfrac{J}{K_m} \ddot{\theta} + \dfrac{B}{K_m} \dot{\theta} + \dfrac{T_L}{K_m}) \\[2mm] \omega_e = \dfrac{d\theta}{dt} \end{cases}$$

(11)

From equations (7) and (11), the PMSM servo system is a flat system, which can be converted to a linear system using a particular internal feedback. Thus, the PMSM servo system can be controlled considerably.

III. PARAMTER IDENTIFITION MODEL OF PMSM BASED ON CEKF

A. PARAMETER ESTIMATION BASED ON CONSENSUS EXTENDED KALMAN FILTER (EKF)

The Kalman filter (KF) algorithm was proposed by Kalman in 1960 based on the principle of linear unbiased minimum variance estimation [26]. The mean square matrix of the filtering error of the KF algorithm can be obtained directly from the algorithm. The extended Kalman filter (EKF) is an improved Kalman filter algorithm for nonlinear systems [27], which is a direct extension of the KF algorithm from linear to nonlinear systems. It linearizes the nonlinear model in real time using the Taylor linear approximation centred on the predicted state. Hence, the KF is used to estimate the state of the system.

According to [28] and [29], the EKF algorithm is suitable for the estimation of systems with constant parameters. It is not suitable for systems with time-varying or mutation parameters. Furthermore, in the EKF algorithm, the nonlinear system function must be locally linearized, thereby resulting in linearization errors. It ignores the linearization error and cannot obtain the mean square matrix of the filtering error. Thus, it cannot directly obtain the bound of the filtering error. In some cases, the filtering value of the EKF algorithm does not converge. The state observation and measurement equations of the nonlinear system are as follows:

$$\begin{cases} \dot{x}(t) = f(x(t), u(t), t) + w(t) \\ y(t) = g(x(t), t) + v(t) \end{cases} \qquad (12)$$

where $x(t)$ is an n-dimensional observed state variable, $y(t)$ an m-dimensional measurement variable, $f(x(t), u(t), t)$ and $g(x(t), t)$ the nonlinear functions with respect to $x(t)$, $w(t)$ and $v(t)$ the zero-mean white noises, with variance matrices $Q(t)$ and $R(t)$, respectively. Their statistical properties are expressed as follows:

$$E[w(t)w^T(\tau)] = Q(t)\delta(t - \tau)$$
$$E[v(t)v^T(\tau)] = R(t)\delta(t - \tau)$$
$$E[w(t)v^T(\tau)] = 0 \qquad (13)$$

where $\delta(t - \tau)$ is a unit pulse function, $Q(t)$ a symmetric nonnegative definite matrix and $R(t)$ a positive definite symmetric matrix. Status $x(t)$, the initial state of $x(t_0)$ is a Gaussian random vector, assuming $x(t_0)$. Here, the mathematical expectation of $E[x(t_0)] = m$ and its variance matrix $P(t_0) = E\left[(x(t_0) - m)(x(t_0) - m)^T\right]$ are known. Further, equation (12) can be transformed into a discrete system as follows:

$$\begin{cases} x(k+1) = x(k) + f(x(k), u(k))\tau + W(k) \\ y(k) = g(x(k)) + v(k) \end{cases} \quad (14)$$

where $W(k) = \phi(k) + w(k)$, τ is the sampling period and $\phi(k)$ the discretization error.

For the general nonlinear system (14), the CEKF algorithm can be expressed as

$$\begin{cases} \bar{x}(k+1) = \hat{x}(k) + f(\hat{x}(k), u(k))\tau \\ \bar{P}_{k+1} = F_k \hat{P}_k F_k^T + Q_k + \Delta Q_k \\ K_{k+1} = \bar{P}_{k+1} H_{k+1}^T (H_{k+1}\bar{P}_{k+1}H_{k+1}^T + R_{k+1})^{-1} \\ \hat{x}(k+1) = \bar{x}(k+1) + K_{k+1}(y(k+1) - g(\bar{x}(k+1))) \\ \hat{P}_{k+1} = (I - K_{k+1}H_{k+1})\bar{P}_{k+1}(I - K_{k+1}H_{k+1})^T \\ \quad\quad + K_{k+1}R_{k+1}K_{k+1}^T + \Delta R_{k+1} \end{cases} \quad (15)$$

where

$$\begin{aligned} \Delta Q_k \geq &-E(F_k(\hat{x}(k) - x(k))\zeta_k^T) - E(\zeta_k(\hat{x}(k) - x(k))^T F_k^T) \\ &+ E(\zeta_k \zeta_k^T) + E(F_k(\hat{x}(k) - x(k))(\hat{x}(k) - x(k))^T F_k^T) \\ &- F_k \hat{P}_k F_k^T \end{aligned} \quad (16)$$

$$\begin{aligned} \Delta R_k \geq &E((I - K_k H_k)(\bar{x}(k) - x(k))\xi_k^T K_k^T) \\ &+ E(K_k \xi_k (\bar{x}(k) - x(k))^T (I - K_k H_k)^T) \\ &+ K_k E(\xi_k \xi_k^T) K_k^T \\ &+ E(K_k v_k v_k^T K_k^T) - K_k R_k K_k^T \\ &+ E((I - K_k H_k)(\bar{x}(k) - x(k))(\bar{x}(k) - x(k))^T \\ &\times (I - K_k H_k)^T) \\ &- (I - K_k H_k)\bar{P}_k(I - K_k H_k)^T \end{aligned} \quad (17)$$

where ζ_k and ξ_k are the linearization errors of the observed state equation and measurement equation, respectively. Here, the conventional EKF ΔQ_k, ΔR_k, is assumed as 0, while the linearization errors ζ_k and ξ_k are neglected. The consistency of the EKF prediction and filtering cannot be guaranteed, thereby resulting in inaccurate filtering results, even divergence and non-convergence. The CEKF algorithm ensures that $E((\hat{x}(k) - x(k))(\hat{x}(k) - x(k))^T) \leq \hat{P}_k$, $k = 0, 1, 2, \ldots$.

B. PMSM PARAMETER IDENTIFICATION MODEL
The voltage equation of the PMSM in the d-q rotating coordinate system is expressed as follows:

$$\begin{cases} u_d = R_s i_d + \dfrac{d\psi_d}{dt} - \omega_r \psi_q \\ u_q = R_s i_q + \dfrac{d\psi_q}{dt} + \omega_r \psi_d \end{cases} \quad (18)$$

where $\begin{cases} \psi_d = L_d i_d + \psi_r \\ \psi_q = L_q i_q \\ \omega_r = n_p \omega_e \end{cases}$.

Thus, the equation can be transformed into:

$$\begin{cases} \dfrac{di_d}{dt} = \dfrac{1}{L_d}u_d - \dfrac{R_s}{L_d}i_d + \dfrac{L_q}{L_d}\omega_r i_q \\ \dfrac{di_q}{dt} = \dfrac{1}{L_q}u_q - \dfrac{R_s}{L_q}i_q - \dfrac{L_d}{L_q}\omega_r i_d - \dfrac{1}{L_q}\omega_r \psi_r \end{cases} \quad (19)$$

where ψ_r is the flux linkage of the permanent magnet of the PMSM, a constant measured in Weber (Wb or V/rad/s). It represents the induction of the stator winding in the permanent magnet, and can be obtained through the voltage constant of the PMSM. The voltage constant K_e refers to the peak value of the line-to-line voltage induced by the stator winding of the PMSM when the motor speed is 1000 rpm, which is converted into an effective value of $\frac{K_e}{\sqrt{3}}$.

ψ_r is calculated as follows:

$$\begin{aligned} \psi_r &= \frac{K_e}{\sqrt{3}}(V/krpm) \\ &= K_e\Big/(\sqrt{3} \times 1000 \times p_n \times pi/30)(V/rad/s) \\ &= \frac{\sqrt{3}\,K_e}{100 \cdot p_n \cdot pi}(Wb). \end{aligned} \quad (20)$$

where p_n is the number of permanent magnet pole pairs of the PMSM. Additionally, ψ_r can also be calculated using the moment constant K_t as follows: $\psi_r = \frac{\sqrt{2}\,K_t}{3 \cdot p_n}(Wb)$. Hence, the spatial state variable equation is expressed as follows:

$$\frac{d}{dt}\begin{bmatrix} i_d \\ i_q \\ R_s \\ L_d \\ L_q \end{bmatrix} = \begin{bmatrix} -\frac{R_s}{L_d} & \frac{L_q}{L_d}\omega_r & 0 & 0 & 0 \\ -\frac{L_d}{L_q}\omega_r & -\frac{R_s}{L_q} & 0 & 0 & 0 \\ 0 & 0 & 0 & 0 & 0 \\ 0 & 0 & 0 & 0 & 0 \\ 0 & 0 & 0 & 0 & 0 \end{bmatrix}\begin{bmatrix} i_d \\ i_q \\ R_s \\ L_d \\ L_q \end{bmatrix}$$
$$+ \begin{bmatrix} \frac{1}{L_d} & 0 \\ 0 & \frac{1}{L_q} \\ 0 & 0 \\ 0 & 0 \\ 0 & 0 \end{bmatrix}\begin{bmatrix} u_d \\ u_q - \omega_r \psi_r \end{bmatrix} \quad (21)$$

The measurement equation is expressed:

$$\begin{bmatrix} i_d \\ i_q \end{bmatrix} = \begin{bmatrix} 1 & 0 & 0 & 0 & 0 \\ 0 & 1 & 0 & 0 & 0 \end{bmatrix}\begin{bmatrix} i_d \\ i_q \\ R_s \\ L_d \\ L_q \end{bmatrix} \quad (22)$$

Suppose τ is the sampling period, and the following difference equation is obtained after discretisation:

$$\begin{cases} x(k+1) = x(k) + f(x(k))\tau + w(k) \\ y(k) = g(x(k)) + v(k) \end{cases} \quad (23)$$

where

$$f(x(k)) = \begin{bmatrix} -\frac{R_s}{L_d} & \frac{L_q}{L_d}\omega_r & 0 & 0 & 0 \\ -\frac{L_d}{L_q}\omega_r & -\frac{R_s}{L_q} & 0 & 0 & 0 \\ 0 & 0 & 0 & 0 & 0 \\ 0 & 0 & 0 & 0 & 0 \\ 0 & 0 & 0 & 0 & 0 \end{bmatrix} x(k)$$

$$+ \begin{bmatrix} \frac{1}{L_d} & 0 \\ 0 & \frac{1}{L_q} \\ 0 & 0 \\ 0 & 0 \\ 0 & 0 \end{bmatrix} \begin{bmatrix} u_d \\ u_q - \omega_r\psi_r \end{bmatrix} \quad (24)$$

$$x(k) = \begin{bmatrix} i_d & i_q & R_s & L_d & L_q \end{bmatrix}^T \quad (25)$$

$$g(x(k)) = \begin{bmatrix} 1 & 0 & 0 & 0 & 0 \\ 0 & 1 & 0 & 0 & 0 \end{bmatrix} x(k) \quad (26)$$

$$y(k) = \begin{bmatrix} i_d \\ i_q \end{bmatrix} \quad (27)$$

By substituting the initial values, parameters and transfer matrix into (15), the online identification model of the PMSM can be obtained.

IV. CURRENT CONTROL ALGORITHM BASED ON ADRC

This study aims to design a servo system for a surface-mounted PMSM. The control strategy is based on the maximum torque method of ID = 0 and space voltage vector control technology based on the principle of field-oriented control. The electromagnetic torque control of the PMSM is realized by controlling the IQ torque current. The current loop control enables the motor stator current to track the motor stator current reference value by controlling the stator voltage. The current loop is the innermost loop of the servo control system, which plays a key role in improving the dynamic performance and control accuracy of the servo system.

A. ESF-BASED PADRC

In the application of fixed sampling frequency, the performance of the controller can be improved by reducing the delay between obtaining the system output signal and refreshing the output signal of the controller (also known as the system input signal) within the sampling period. The input and output delay do not necessarily depend on the calculation complexity of the controller algorithm but on the necessary calculation required to obtain the controller output. Hence, the complex calculation can be placed into the remaining time of the sampling period after the controller output is considerably refreshed. As such, we proposed an EPADRC control technology with prediction and later correction. Consider the nth-order nonlinear time-varying uncertain system

as expressed below:

$$\begin{cases} \dot{x} = A_C x + B_c f(x, w, t) + B_{uc} u \\ y = C_d x \end{cases} \quad (28)$$

where

$$A_c = \begin{bmatrix} 0 & 1 & 0 & \cdots & 0 \\ 0 & 0 & 1 & \cdots & 0 \\ \vdots & & & \ddots & \\ 0 & 0 & 0 & \cdots & 1 \\ 0 & 0 & 0 & \cdots & 0 \end{bmatrix}, B_c = \begin{bmatrix} 0 \\ 0 \\ 0 \\ \vdots \\ 1 \end{bmatrix},$$

$$B_{uc} = \begin{bmatrix} 0 \\ 0 \\ 0 \\ \vdots \\ b \end{bmatrix}, C_d = \begin{bmatrix} 1 & 0 & 0 & \cdots & 0 \end{bmatrix}.$$

This is a continuous-time system where x is a continuous state variable $x = [x_1, x_2, \cdots, x_n]$ and y the system output. The corresponding EPADRC loop iteration algorithm is expressed as follows:

$$\begin{cases} K_k = -AP_k C^T \left(CP_k C^T + \frac{R_k}{1+\theta} \right)^T \\ P_{k+1} = (1+\theta)(A + K_k C) P_k (A + K_k C)^T \\ + K_k R_k K_k^T + \frac{1+\theta}{\theta} Q_k \\ Q_k = 2 \begin{bmatrix} Q_{1k} & 0 \\ 0 & Q_{2k} \end{bmatrix}, Q_{1k} = q_{1,k}{}^2, Q_{2k} = q_{2,k}^2 \\ \tilde{L}_E = -T^{-1} K_k \end{cases} \quad (29)$$

where

$$P_0 \geq E[(X_k - z_k)(X_k - z_k)^T],$$

$$X_k = (x_{1,k}, x_{2,k}, \cdots, x_{n,k}, f_k)^T$$

$$R_k \geq E(n_k n_k^T)$$

$$q_{1,k,i} \geq |w_{k,i}|, i = 1, 2, \cdots, n$$

$$q_{2,k} \geq |f_{k+1} - f_k|\theta > 0$$

$$\hat{\bar{G}}_k \overset{\Delta}{=} sat(\tilde{G}_k, q_{2,k}), \tilde{G}_k \overset{\Delta}{=} \bar{G}(\hat{x}_k, k\tau), \hat{f}_0 = \hat{\bar{f}}_0.$$

The structure of the EPADRC is shown in figure 1 as shown below:
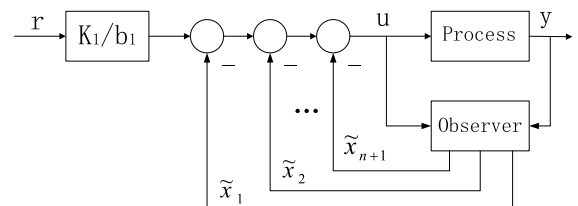

FIGURE 1. Improved ADRC structure diagram.

B. CURRENT CONTROL ALGORITHM

Owing to the adoption of $i_d = 0$, the control strategy realizes the decoupling of torque current i_q and stator field current i_d. From the first equation of equation (7), suppose the control input is u_d and the system state variables i_d, a PMSM can be obtained. The differential equation for the current loop state space is expressed as follows:

$$\begin{cases} \dot{i}_d = \dfrac{1}{L_d}(n_p\omega_e L_q i_q - R_s i_d) + \dfrac{1}{L_d}u_d \\ y = i_d + n_{dk} \end{cases} \quad (30)$$

The motor parameters identified using the CEKF are resistance, q-, and d-axis inductance, that is, $\hat{R}_s, \hat{L}_q, \hat{L}_d$, respectively.

$$f(i_d, t) = \frac{1}{L_d}(n_p\omega_e L_q i_q - R_s i_d)$$

$$\dot{f}(i_d, t) = \frac{1}{L_d}(n_p a L_q i_q + n_p\omega_e L_q \dot{i}_q - R_s \dot{i}_d)$$

$$\hat{f}(i_d, t) = \frac{1}{\hat{L}_d}(n_p\omega_e \hat{L}_q i_q - \hat{R}_s i_d)$$

$$\delta(i_d, t) = f(i_d, t) - \hat{f}(i_d, t) + (\frac{1}{L_d} - \frac{1}{\hat{L}_d})u_d$$

Thus, i_d in the differential equation (31) for the current loop state space can be transformed to:

$$\begin{cases} \dot{i}_d = \hat{f}(i_d, t) + \delta(i_d, t) + \dfrac{1}{\hat{L}_d}u_d \\ y = i_d + n_{dk} \end{cases} \quad (31)$$

Assuming $\hat{f}(i_d, t)$ is the known part of the model, $\delta(i_d, t)$. The unknown nonlinear part of the system is considered as the total disturbance. The system gain factor $b = \frac{1}{\hat{L}_d}$.

The standard form of the extended state differential equation corresponding to the state equation (32) is expressed as follows:

$$\begin{cases} \dot{x} = Ax + B\left(u_d + \hat{f}(i_d, t) \cdot \hat{L}_d\right) = Ax + Bu_0 \\ y = Cx + n_{dk} \end{cases} \quad (32)$$

where $x = \begin{bmatrix} i_d \\ \delta(i_d, t) \end{bmatrix}$, $A = \begin{bmatrix} 0 & 1 \\ 0 & 0 \end{bmatrix}$, $B = \begin{bmatrix} \frac{1}{\hat{L}_d} \\ 0 \end{bmatrix}$ and $C = [1 0]$. Here, the ID current setting is $r = 0$

The coefficient matrices A, B and C of equation (33), initial state variable x and output direct current axis detected by the PMSM current sensor y can be substituted into the EPADRC anti-interference algorithm to perform periodic cyclic

iteration operation as expressed as follows:

$$\begin{cases} \begin{cases} u_k = \bar{u}_k - (\tilde{l}_1 + \tilde{l}_2)y_k \\ \bar{x}_{k+1} = \tilde{A}_E(\bar{x}_k + \tilde{L}_E y_k) + \tilde{B}_E u_k \\ \bar{u}_{k+1} = k_1 \hat{L}_d r_{k+1} - [11]\bar{x}_{k+1} \end{cases} \\ \begin{cases} K_k = -AP_k C^T\left(CP_k C^T + \dfrac{R_k}{1+\theta}\right)^T \\ P_{k+1} = (1+\theta)(A+K_kC)P_k(A+K_kC)^T \\ \qquad + K_k R_k K_k^T + \dfrac{1+\theta}{\theta}Q_k \\ Q_k = 2\begin{bmatrix} Q_{1k} & 0 \\ 0 & Q_{2k} \end{bmatrix}, Q_{1k} = q_{1,k}^2, Q_{2k} = q_{2,k}^2 \\ \tilde{L}_E = -T^{-1}K_k \\ T^{-1} = \hat{L}_d\begin{bmatrix} k_1 & 0 \\ 0 & 1 \end{bmatrix}, \tilde{L}_E = \begin{bmatrix} \tilde{l}_1 \\ \tilde{l}_2 \end{bmatrix} \\ A_E = A + K_kC, B_E = B, L_E = -K_k \\ \tilde{A}_E = T^{-1}A_E T, \tilde{B}_E = T^{-1}B_E, \tilde{L}_E = T^{-1}L_E \end{cases} \end{cases}$$

(33)

where $R_k \geq E(n_{dk}n_{dk}^T)$, $q_{1,k} \geq |w_k|$ and $q_{2,k} \geq |\delta_{k+1} - \delta_k|$.

u_k is the output action of (33) and u_0 the actual control output of the system in (31). u_d is the direct axis voltage of the PMSM expressed as

$$u_d = u_k - \hat{f}(i_d, t) \cdot \hat{L}_d \quad (34)$$

where i_d is the output action of the current loop EPADRC. Additionally, i_d can be considered the current loop control algorithm.

V. EXPERIMENT AND RESULT ANALYSIS

A. EXPENIMENTAL ENVIROMENT

The experiment is based on the self-made two-axis two-frame servo control system, and the system control block diagram is shown in figure 2. The CPU of the main board is TMS320F28335 floating-point DSP, and an experimental test is conducted on a six-degree-of-freedom platform under the working environment of the analogue servo control system. Under this carrier, the EPADRC with and without parameter identification are also compared in current control experiments.

The permanent magnet servo system must have a fast dynamic response and high steady-state accuracy. The current loop, as the innermost loop of the servo system, is the foundation for ensuring the overall system performance. However, factors such as disturbances in the current loop and control delays caused by digital control will have adverse effects on the control performance. This experiment adopts the parameter identification method of consistency EKF, which can effectively improve the dynamic characteristics and robustness of the system.
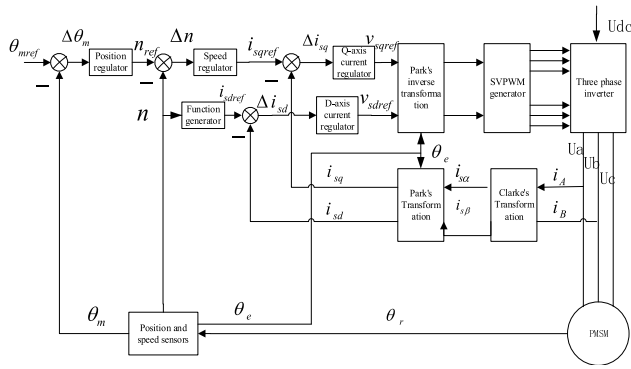
FIGURE 2. PMSM servo control block diagram.

B. PARAMETER IDENTIFICATION EXPERIMENT

EGK65-60NCB manufactured by Geshuo Electric Co., Ltd. in Germany is used in the PMSM servo syetem. The number of pole pairs is 10. The main motor parameters are as follows: voltage constant $K_e = 68V/1000 \min^{-1}$ and moment constant $K_t = 1.12Nm/A$. The permanent magnet flux linkage can be calculated from the voltage constant of the PMSM as expressed below:

$$\psi_r = \frac{K_e}{\sqrt{3}}(V/krpm)$$
$$= K_e / (\sqrt{3} \times 1000 \times p_n \times pi/30)(V/rad/s)$$
$$= \frac{\sqrt{3} K_e}{100 \cdot p_n \cdot pi}(Wb) \qquad (35)$$

The output of the simulated motor can be obtained using the motor model. i_d, i_q, u_d, u_d and ω_r. In the CEKF algorithm, the initial values of P, Q, and R are expressed as follows:

$P = diag([0.1\ 0.1\ 0.0003\ 0.001\ 0.001])$,
$R = diag([0.1\ 0.2])$.
$Q_k = \beta_k \cdot \beta_k^T$

where $\beta_k = \frac{\tau^2}{2}\frac{df}{dt}(\tilde{x}_k), \tilde{x}_k \in (x(k), x(k+1))$.

Because the measurement equation is linear and state equation is nonlinear,

$$\Delta R_k = 0;$$
$$\Delta Q_k = \alpha_{Q,k}\Delta Q_{P,k} + \frac{\Delta Q_{\phi,k}}{\alpha_{Q,k}} + \Delta Q_{\phi,k}$$

where

$$\alpha_{Q,k} = \sqrt{\frac{\|\Delta Q_{\phi,k}\|}{\|\Delta Q_{P,k}\|}}, \Delta Q_{P,k} = F_k \hat{P}_k F_k^T,$$
$$\Delta Q_{\phi,k} = 3diag(\phi_{k,1}^2, \phi_{k,2}^2, \phi_{k,3}^2, \phi_{k,4}^2, \phi_{k,5}^2),$$
$$\phi_{k,i} = \frac{1}{2}trace([\frac{d^2f_i}{dx}|\hat{x}(k)] \cdot \hat{P}_k), i = 1, 2, \cdots, 5$$

The proposed EKF and CEKF algorithms are used to identify the motor parameters, thereby leading to the obtention of the required parameters $(R_s\ L_d\ L_q)$ of the PMSM. The simulation results are as follows:
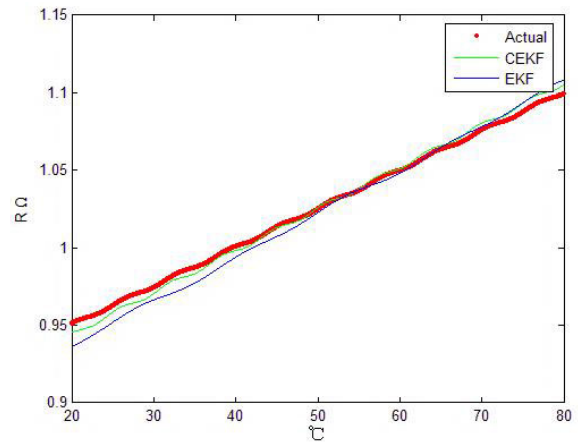

FIGURE 3. Simulation of EKF and CEKF estimation of resistance Rs.

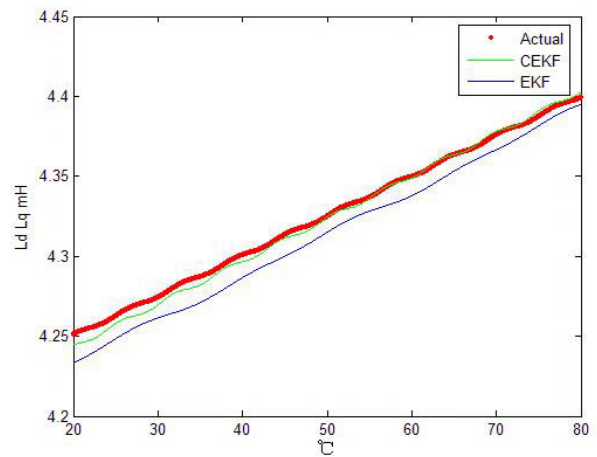**FIGURE 4. Simulation of estimation of inductance Ld and Lq using EKF and CEKF.**

TABLE 1. Mean square value of the identification error of the CEKF and EKF algorithms.

	CEKF	EKF
R_s (Ω)	0.0137	0.0208
L_s (mH)	0.0102	0.0284

As shown in figures 3 and 4 and Table 1, when the resistance and inductance change in a small range, the identification result error of the CEKF is small, and its identification effect is better than that of EKF. Additionally, the EKF is suitable for the parameter identification of the system with constant parameters. Meanwhile, because the conventional EKF cannot guarantee the convergence of the estimated value, the algorithm can diverge.

Although L_d and L_q do not change with a change in speed, they decrease with an increase in torque. i_d and i_q also change similarly. Further, the resistance and inductance parameters of the motor are time-varying with a change in motor temperature. Because the CEKF uses linear error

compensation, it has more advantages in terms of the parameter identification.

C. ANALYSIS OF EXPERIMENTAL RESULTS OF PMSM CURRENT CONTROL

(1) Accuracy Test of the Current Loop of a PMSM Based on the EPADRC Technology

The current loop parameters of the servo system azimuth frame PMSMs are a torque current setting value of $i_{qs} = 0.5 \cdot sign(\sin 2\pi t)$, square wave with an amplitude of 0.5 A, period of 1000 ms and d-axis current setting value $i_{qs} = 0$. The PMSM current sensor output of the phase current waveforms of i_a and i_b are shown in figures 5–8. A comparison of the actual output current waveform of i_a and i_b in the d–q coordinate system obtained by the park transformation of i_q and i_d is shown in figure 5. As shown in figure 6, the actual output current i_q, i_d maintains a good track of set i_{qs}, i_{ds}, wherein the tracking error of i_q is ± 10 mA and that of i_d is ± 15 mA.

The current loop parameters of the servo system pitch frame PMSM are: a torque current setting value of $i_{qs} = 0.6 \cdot sign(\sin 2\pi t)$, square wave with an amplitude of 0.6 A, period of 1000 ms and d-axis current setting value of $i_{qs} = 0$. The phase current waveforms of the PMSM current sensor output i_a and i_b are shown in figures 5–6. A comparison of the actual output current waveform of i_a and i_b in the d–q coordinate system obtained using the park transformation of i_q and i_d is shown in figure 7. As shown in figure 8, the actual output current i_q, i_d maintains a good track of set i_{qs}, i_{ds}, wherein the tracking error of i_q is ± 15 mA, and that of i_d is ± 20 mA.
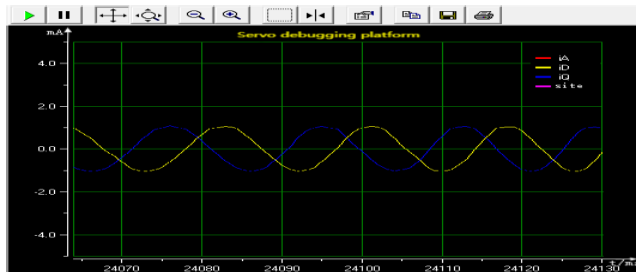

FIGURE 5. Current waveform of phases ia and ib of the Azimuth motor of the photoelectric stabilised tracking platform.

(2) Current Loop Comparison Experiment of the PMSM with the EPADRC and Conventional ADRC Control Technology

The experimental results of the EPADRC current loop with a parameter identification function under a torque current setting of $i_{qs} = 0.8 \cdot sign(\sin 2\pi t)$ is shown in figure 9. The experimental results of the EPADRC current loop without the parameter identification function under a similar torque current setting condition are shown in figure 10.

The experimental results of the EPADRC current loop with a parameter identification function under a torque current setting of $i_{qs} = 1.2 \cdot sign(\sin 2\pi t)$ is shown in figure 11. The experimental results of the EPADRC current loop without

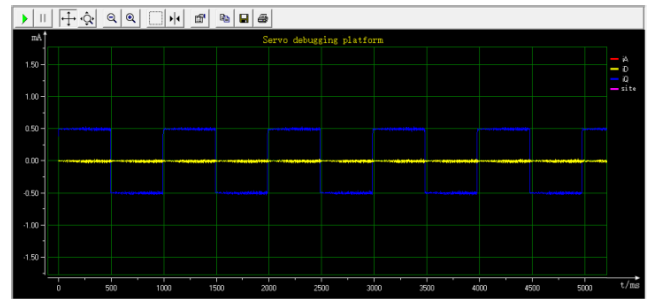**FIGURE 6.** ID and IQ current tracking waveforms of an Azimuth motor of an electro-optical stabilised tracking platform.
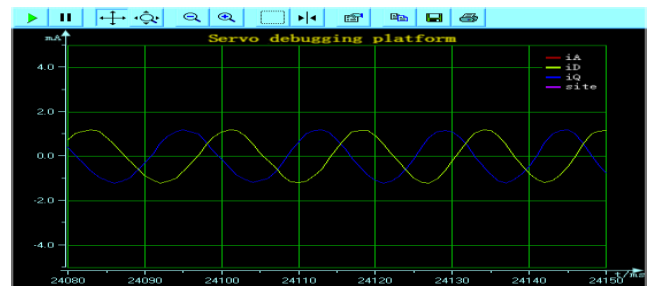

FIGURE 7. Current waveforms of phases ia and ib of the elevation motor of an electro-optical stabilised and tracking platform.
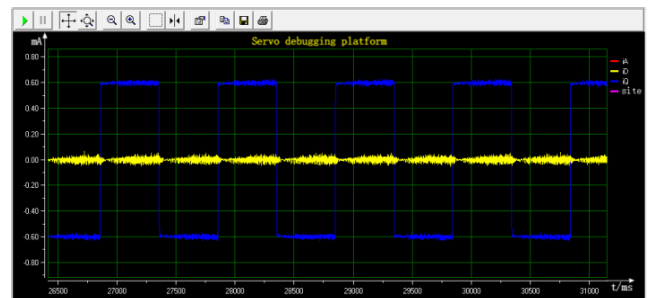

FIGURE 8. ID and IQ current tracking waveforms of the elevation motor of an electro-optical stabilised and tracking platform.
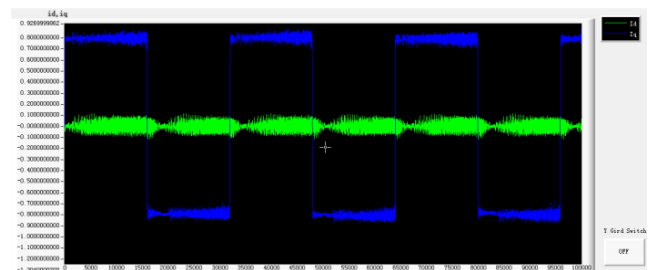

FIGURE 9. The ID and IQ current tracking waveforms of the Azimuth frame with a parameter identification function (IQ = 0.8 A).

a parameter identification function under a similar torque current setting are shown in figure 12.

From the comparative analysis of figures 9–12, it can be deduced that the current loop PMSM based on the EPADRC control technology outputs the ID, an IQ current with minor
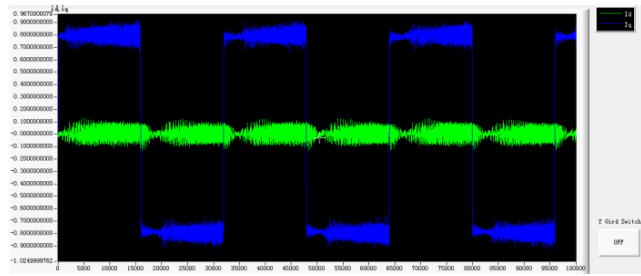
FIGURE 10. The ID and IQ current tracking waveforms of the EPADRC Azimuth frame without the parameter identification function (IQ = 0.8A).
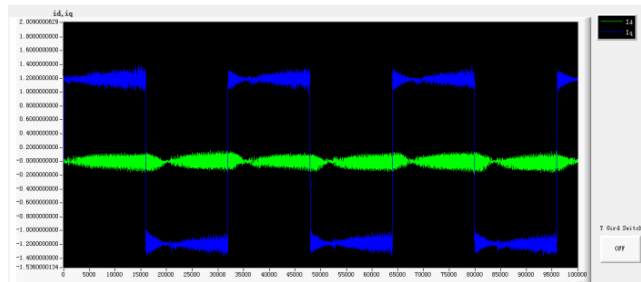

FIGURE 11. The ID and IQ current tracking waveforms of the EPADRC Azimuth frame with the parameter identification function (IQ = 1.2 A).
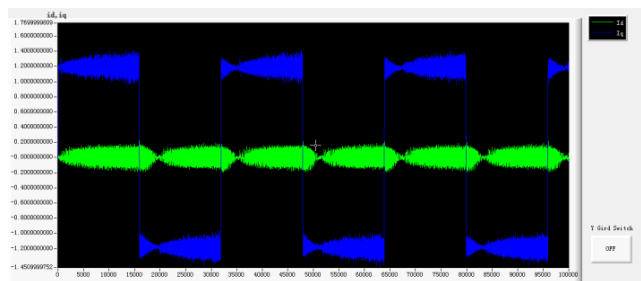

FIGURE 12. The ID and IQ current tracking waveform of the EPADRC Azimuth frame without the parameter identification function (IQ = 1.2 A).

fluctuations, and little influence of the random noise. Based on the experiment, EPADRC has a strong filtering function and improves the control accuracy.

VI. CONCLUSION

This study proposed a current loop control method with a parameter identification function for a PMSM servo system, and the effectiveness of the proposed method was validated through servo control experiments. The following conclusions can be drawn from this study:

(1) A PMSM servo system can be equivalent to a linear system by using a special type of internal feedback. Thus, the PMSM servo system can be controlled considerably.

(2) The CEKF considered the existence of the system linearization error and took it as the mean square matrix of the filter error to participate in the CEKF recursive operation, which ensured the consistency and convergence of the identification value.

(3) The proposed method was characterized by active filtering, tracking, disturbance rejection, and prediction. Further, it is suitable for the control of high precision and dynamic response of nonlinear, strong coupling systems, and systems with large-scale uncertain disturbance.

REFERENCES

[1] J. Gao, S. Zhao, F. Jiang, W. Du, and Z. Zheng, "A novel hollow two-sided output PMSM integrated with mechanical planetary gear: A solution for drive and transmission system of servo press," *IEEE/ASME Trans. Mechatronics*, vol. 27, no. 5, pp. 3076–3086, Oct. 2022.

[2] D. Lyu, Q. Liu, H. Liu, and W. Zhao, "Dynamic error of CNC machine tools: A state-of-the-art review," *Int. J. Adv. Manuf. Technol.*, vol. 106, nos. 5–6, pp. 1869–1891, Jan. 2020.

[3] X. H. Luo, J. Y. Jin, J. H. Kong, X. P. Yang, and J. X. Chen, "Spectral-domain model of PMSM vector control system and its application," *J. Donghua Univ.*, vol. 48, no. 5, pp. 84–90, 2022.

[4] Q. D. Guo, Y. B. Sun, and L. M. Wang, *Modern Permanent Magnet Motor AC Servo System*. Beijing, China: China Electric Power Press, 2006.

[5] L. Zhong and M. F. Rahman, "Analysis of direct torque control in permanent magnet synchronous motor drives," *IEEE Trans. Power Electron.*, vol. 12, no. 3, pp. 528–536, May 1997.

[6] H. Takami, "Robust current control for permanent magnet synchronous motors by the inverse LQ method—An evaluation of control performance using servo-locks at low speed," *J. Power Electron.*, vol. 4, no. 4, pp. 228–236, 2004.

[7] F. X. Wang, Z. H. Ke, D. L. Ke, and C. G. Hu, "Model-free predictive current control of three-level inverter-fed PMSM based on strong tracking extended Kalman observer," (in Chinese), *Proc. CSEE*, to be published.

[8] R. Errouissi, M. Ouhrouche, W.-H. Chen, and A. M. Trzynadlowski, "Robust nonlinear predictive controller for permanent-magnet synchronous motors with an optimized cost function," *IEEE Trans. Ind. Electron.*, vol. 59, no. 7, pp. 2849–2858, Jul. 2012.

[9] Y. He, J. Liu, Z. Wang, and Y. Zou, "A PI control algorithm with zero static misadjustment for tracking the harmonic current of three-level APFs," *J. Power Electron.*, vol. 14, no. 1, pp. 175–182, Jan. 2014.

[10] C. Ogbuka, C. Nwosu, and M. Agu, "A high performance hysteresis current control of a permanent magnet synchronous motor drive," *TURKISH J. Electr. Eng. Comput. Sci.*, vol. 25, pp. 1–14, Jan. 2017.

[11] Y. Deng, J. Wang, H. Li, J. Liu, and D. Tian, "Adaptive sliding mode current control with sliding mode disturbance observer for PMSM drives," *ISA Trans.*, vol. 88, pp. 113–126, May 2019.

[12] C. L. Wang, D. X. Cao, X. X. Qu, and H. Hu, "Predictive current control for a two-phase hybrid stepper motor fed by a three-phase voltage source inverter," *Electr. Mach. Control*, vol. 25, no. 12, pp. 27–35, 2021.

[13] O. Lopez-Santos, D. S. Dantonio, F. Flores-Bahamonde, and C. A. Torres-Pinzon, "Hysteresis control methods," in *Multilevel Inverters*. Cambridge, MA, USA: Academic Press, 2021, pp. 35–60.

[14] F. Mou, D. Wu, and Y. Dong, "Disturbance rejection sliding mode control for robots and learning design," *Intell. Service Robot.*, vol. 14, no. 2, pp. 251–269, Apr. 2021.

[15] C. A. Busada, S. G. Jorge, and J. A. Solsona, "A synchronous reference frame PI current controller with dead beat response," *IEEE Trans. Power Electron.*, vol. 35, no. 3, pp. 3015–3097, Mar. 2020.

[16] R. Errouissi and A. Al-Durra, "Decoupled PI current controller for grid-tied inverters with improved transient performances," *IET Power Electron.*, vol. 12, no. 2, pp. 245–253, Feb. 2019.

[17] T. Zhao, Z. B. Liao, and Z. D. Wang, "High response current loop control of AC servo system," *J. Huaqiao Univ.*, vol. 41, no. 3, pp. 374–380, 2020.

[18] Y. Huang and W. C. Xue, "Active disturbance rejection control: Methodology," *Appl. Theor. Anal.*, vol. 32, no. 10, pp. 1287–1307, 2012.

[19] B. W. Zhang, "Analysis, design and tuning of active disturbance rejection control," Ph.D. thesis, North China Electr. Power Univ., Beijing, China, 2021.

[20] S. Y. Shi, S. P. Zhao, and J. Li, "On tracking ability analysis of linear extended state observer for uncertain system," *Comput. Model. New Technol.*, vol. 18, no. 2, pp. 175–179, 2014.

[21] G. Battistelli and L. Chisci, "Stability of consensus extended Kalman filter for distributed state estimation," *Automatica*, vol. 68, pp. 169–178, Jun. 2016.

[22] S. Shi, Z. Zeng, C. Zhao, L. Guo, and P. Chen, "Improved active disturbance rejection control (ADRC) with extended state filters," *Energies*, vol. 15, no. 16, p. 5799, Aug. 2022.

[23] H. Sira-Ramirez, J. Linares-Flores, C. Garcia-Rodriguez, and M. A. Contreras-Ordaz, "On the control of the permanent magnet synchronous motor: An active disturbance rejection control approach," *IEEE Trans. Control Syst. Technol.*, vol. 22, no. 5, pp. 2056–2063, Sep. 2014.

[24] J. P. Louis, *Control of Synchronous Motors*. New York, NY, USA: Wiley, 2011.

[25] M. Fliess, J. Lévine, P. Martin, and P. Rouchon, "Flatness and defect of non-linear systems: Introductory theory and examples," *Int. J. Control*, vol. 61, no. 6, pp. 1327–1361, Jun. 1995.

[26] R. E. Kalman, "A new approach to linear filtering and prediction problem," *J. Basic Eng.*, vol. 82, pp. 35–45, Jan. 1960.

[27] S. J. Julier and J. K. Uhlmann, "New extension of the Kalman filter to nonlinear systems," in *Proc. SPIE*, vol. 3068, pp. 182–193, Jul. 1997.

[28] J. Hernandez-Barragan, J. D. Rios, A. Y. Alanis, C. Lopez-Franco, J. Gomez-Avila, and N. Arana-Daniel, "Adaptive single neuron anti-windup PID controller based on the extended Kalman filter algorithm," *Electronics*, vol. 9, no. 4, p. 636, 2020.

[29] M. Valipour and L. A. Ricardez-Sandoval, "Constrained abridged Gaussian sum extended Kalman filter: Constrained nonlinear systems with non-Gaussian noises and uncertainties," *Ind. Eng. Chem. Res.*, vol. 60, no. 47, pp. 17110–17127, Dec. 2021.

LUJI GUO received the B.S. degree in aircraft manufacture engineering from the College of Mechatronic Engineering, North University of China, in 2022, where he is currently pursuing the master's degree with the School of Aeronautics and Astronautics. His research interest includes UAV attitude control.

ZHE CHANG received the B.S. degree in aircraft design and engineering from the College of Mechatronic Engineering, North University of China, in 2020, where she is currently pursuing the master's degree with the School of Aerospace Engineering. Her research interest includes aircraft mechanics and control.

CHENBO ZHAO received the B.S. degree in aircraft manufacture engineering from the College of Mechatronic Engineering, North University of China, in 2021, where he is currently pursuing the master's degree with the School of Aeronautics and Astronautics. His research interest includes UAV attitude control.

SHANGYAO SHI received the Ph.D. degree in measurement technology from Sichuan University, in 2016. He developed China's first DC frequency conversion air conditioning controller, and the developed DC frequency conversion air conditioning products won the Sichuan Innovation Achievement, in 1999, and received the Award, in 2000. From 2002 to 2004, he was engaged in the network control system design and system implementation of the national giant laser fusion device—Shenguang-III with the China Academy of Engineering Physics. From 2004 to 2009, he was the Chief Engineer of Guangdong Leiqi Optoelectronics Company Ltd. From 2009 to 2012, he was the Director of Servo and Power Room with Sichuan Electronics Military Industry Group, engaged in the research and development of airborne photoelectric radar servo control system of J-XX fighter aircraft; From 2012 to 2017, he was the Chief Engineer of core subsidiary with Huagong Technology Industry Company Ltd. He joined the North University of China, in 2018, and is currently a Professor-Level Senior Engineer with the School of Software. His research interests include intelligent control, machine vision, cluster multi-agent, industrial internet, and digital twin intelligent manufacturing systems.

PENGYUN CHEN received the B.S. and Ph.D. degrees in design and construction of naval architecture and ocean structure from Harbin Engineering University, Harbin, China, in 2010 and 2016, respectively. Since 2016, he has been a Lecturer with the College of Mechatronic Engineering. Since 2020, he has also been an Associate Professor with the North University of China. His research interests include the autonomous control and navigation technology of unmanned vehicle, optical target recognition, and tracking.

• • •